Electron paramagnetic resonance and photochromism of N_3V^0 in diamond

B. L. Green, B. G. Breeze, M. E. Newton

Department of Physics, University of Warwick, Coventry, CV4 7AL, United Kingdom

E-mail: b.green@warwick.ac.uk; m.e.newton@warwick.ac.uk

Abstract. The defect in diamond formed by a vacancy surrounded by three nearest-neighbor nitrogen atoms and one carbon atom, N_3V, is found in the vast majority of natural diamonds. Despite N_3V^0 being the earliest electron paramagnetic resonance spectrum observed in diamond, to date no satisfactory simulation of the spectrum for an arbitrary magnetic field direction has been produced due to its complexity. In this work, N_3V^0 is identified in ^{15}N-doped synthetic diamond following irradiation and annealing. The $^{15}N_3V^0$ spin Hamiltonian parameters are directly determined and used to refine the parameters for $^{14}N_3V^0$, enabling the latter to be accurately simulated and fitted for an arbitrary magnetic field direction. Study of $^{15}N_3V^0$ under excitation with green light indicates charge transfer between N_3V and N_s. It is argued that this charge transfer is facilitated by direct ionization of N_3V^-, an as-yet unobserved charge state of N_3V.

Submitted to: *J. Phys.: Condens. Matter*

1. Introduction

Through careful advances in both processing and particularly synthesis, diamond has become a material with a great variety of technological applications including magnetic bio-imaging [1, 2], thermal management [3, 4, 5], ultra-hard tooling [6] and particle detectors [7]. Underpinning these technological applications have been advances in understanding of defect and impurity properties within diamond, and their behavior during synthesis and processing.

Nitrogen is probably the most common impurity in both natural and synthetic diamond [8]. It is incorporated during high pressure high temperature (HPHT) growth of diamond primarily as single substitutional nitrogen, N_s. Annealing can drive the aggregation of nitrogen into higher-order complexes — the nitrogen-vacancy family N_nV (with $n = 1$–4) and N_s-N_s (a substitutional pair defect, the so-called A-center) [9]. Electron paramagnetic resonance (EPR) and optical signatures have been identified for $NV^{0/-}$ [10, 11, 12], $N_2V^{0/-}$ [13, 14], N_3V^0 [15, 16], and optical-only for N_4V^0 (known as the B-center) [17]. The charge state of each of these defects in nitrogen-rich diamond is defined primarily by the concentration of N_s, which is a donor with an ionization threshold of approximately 1.7 eV [18].

The N3 absorption and luminescence band, with a zero-phonon line (ZPL) at 2.988 eV (415 nm, Fig. 1(c)), is observed in the vast majority of natural diamonds and some treated synthetic diamonds. Indeed, its ubiquity in natural diamond has led to the development of a commercial categorization device which looks for the presence of the absorption band [19]. A complex EPR spectrum, (known as P2, Fig. 1(a)), is associated with the N3 absorption band by correlation between the EPR and optical signatures [15]. Through careful electron nuclear double resonance (ENDOR) experiments, the EPR spectrum was determined to arise at a center containing three nitrogen atoms decorating a vacancy, N_3V^0 (Fig. 1(b)) [20, 16].

The exact production route of N_3V is not known. Calculations on the diffusion of nitrogen indicate that the energy required for concerted exchange is too high (>6.3 eV [21, 22]) to contribute significantly at typical annealing temperatures (400–2200 °C). Aggregation is therefore understood to be mediated by the migration of vacancies [23] and interstitials [24, 25]: the rate of aggregation can be increased by the non-equilibrium introduction of vacancies and interstitials [23], typically by electron irradiation. These two intrinsic defects dictate two distinct classes of aggregation behavior. In the vacancy-driven model, vacancies (which become mobile at >700 °C) migrate to N_s, forming NV. NV can then diffuse by dissociation and subsequent re-capture of the vacancy [26], forming N_2V when two NV centers annihilate and emit a vacancy (1600 °C [27]). At higher temperatures (>1800 °C [28, 9]) N_2V then spontaneously emits a vacancy, forming N_2. On the other hand, the interstitial model describes aggregates in terms of nitrogen interstitials, primarily N_I and N_{2I} [29]. Nitrogen interstitials introduced by irradiation (or converted from C_I by low-temperature annealing [24]) aggregate to N_{2I} at temperatures as low as 650 °C in nitrogen-rich diamond [29]: this complex anneals out at approximately 1500 °C, enabling the reaction $N_{2I} \rightarrow C_I + N_s\text{-}N_s$ [25, 30]. N_2V is subsequently formed by capture of a vacancy at N_s-N_s (>1600 °C). In both models, the route to production of N_3V and N_4V is not clear, though it is speculated that they form by migration and aggregation of lower-order aggregates [25]. It is likely that both the interstitial- and vacancy-mediated aggregation models are viable and operate simultaneously, with the dominant model for a given sample depending strongly on the relative concentrations of different impurities and intrinsic defects.

Once produced, the N_3V structure has C_{3v} symmetry and hence there are four equivalent orientations of the defect within the diamond lattice, each defined by its unique $\langle 1\,1\,1\rangle$ axis. Each nitrogen atom is covalently bonded to its three carbon nearest-neighbors, with its lone pair directed into the vacancy. We therefore expect the unpaired electron probability density to reside primarily on the carbon atom nearest-neighbor to the vacancy, with a commensurately small electron-nuclear hyperfine interaction with each of the nitrogen constituents. Using the vacancy-cage model of electronic structure in diamond (which explicitly deals only with those orbitals pointing in towards the vacancy) [31], the one-electron description of the N_3V^0 ground state is $a_{1N}^2 e_N^4 a_{1C}^1$ (with N and C indicating orbitals located primarily on nitrogen and carbon atoms, respectively), yielding a $^2A_1$ ground state and a ^2E excited state — in this model, only one other high-energy $^2A_1$ state is possible. This

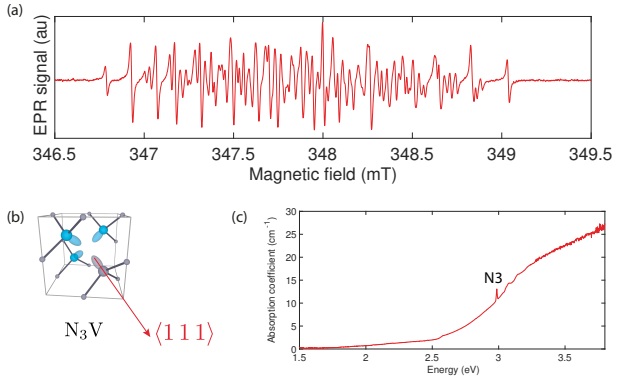

Figure 1. (a) EPR spectrum of a diamond containing $^{14}N_3V^0$, with the applied magnetic field $B\|\langle 0\,0\,1\rangle$. The complex structure is due to electron-nuclear interactions with the three $I = 1$ ^{14}N nuclei. (b) Atomic structure of N_3V in diamond, with the $\langle 1\,1\,1\rangle$ C_{3v} symmetry axis highlighted. (c) UV-Vis absorption spectrum of a synthetic ^{15}N-doped HPHT-grown diamond containing N_3V^0 (ZPL at 2.988 eV) and substitutional nitrogen (N_s^0, absorption ramp starting at approximately 2 eV).

is in stark contrast to NV^-, which possesses the same one-electron symmetry but two fewer electrons and hence can generate a multitude of high-spin ($S > 1/2$) states [12]. The vacancy-cage model may explain the lack of observation of N_3V^-: addition of an electron to N_3V^0 leaves a closed-shell spin singlet with no bound optical transitions, precluding sharp optical transitions and observation by EPR. Nevertheless, some confusion surrounds the precise electronic structure of N_3V^0, with some calculations predicting weakly-bound excitonic-type states [32].

Due to its prevalence in natural diamond, the ability to quantify N_3V^0 concentrations is key in devloping characterization and discrimination tools. The published spin Hamiltonian parameters (see Table 1) produce a satisfactory EPR spectral simulation only for an external magnetic field $B\|\langle 0\,0\,1\rangle$. For all other directions, the published parameters produce a poor simulation: this presents a problem when attempting to quantify defect concentrations in crystals whose orientation is not known, or where experimental geometric constraints prevent the crystal being oriented along $\langle 1\,0\,0\rangle$. As a result of the complexity of the $^{14}N_3V^0$ EPR spectrum (Fig. 1(a)), very small changes to the spin Hamiltonian parameters have a dramatic effect on the quality of a simulation of the measured spectrum. The production of N_3V^0 in a ^{15}N-doped diamond would greatly simplify the observed EPR spectrum (see §2.3) and enable revised spin Hamiltonian parameters to be obtained for higher-accuracy, arbitrary-direction quantification.

Exploiting recent advances in synthesis, we have measured ^{15}N-doped synthetic diamond to determine more accurate spin Hamiltonian parameters for the N_3V^0 EPR center. As a consequence of nitrogen aggregation over geological timescales in natural diamond and the need for stabilizing pressure (>3 GPa) at annealing temperatures above 1600 °C, the significant concentrations (>1 ppm) of both N_3V and the donor N_s in this sample are unusual. We have therefore studied the photochromism behavior of N_3V^0 with a view to confirming the presence of N_3V^-, and to identify any associated optical features.

2. Methods

2.1. Sample

Atmospheric nitrogen is readily incorporated into diamond during HPHT growth if chemical nitrogen traps ("getters") are not employed. The sample used in this experiment was grown using a HPHT growth capsule that was outgassed under vacuum and subsequently backfilled with an isotopically enriched N_s-N_s gas [34] with a nitrogen isotopic ratio of ^{14}N:^{15}N of approximately 5:95 (see [14] for further discussion of synthesis method). A total substitutional nitrogen concentration of 84(3) ppm was measured after growth. The sample was irradiated to a total dose of approximately 5×10^{17} neutrons cm^{-2} under atmospheric conditions at an estimated sample temperature of approximately 200 °C [35] in order to introduce vacancies and interstitials. The sample was then annealed for 15 h at 1500 °C in a non-oxidizing atmosphere to produce N_2V and N_s-N_s, before a further 1 h anneal under HPHT conditions at a nominal temperature of 1900 °C to create N_3V.

After processing the sample was measured (by IR absorption) to contain $^{15}N_s^0 \approx 20$ ppm; $^{15}N_s^+ \approx 5$ ppm; and $(N_s\text{-}N_s)^0 \approx 40$ ppm. The concentrations are approximate as we do not have a suitable reference spectrum for $^{15}N_4V^0$: we estimate approximately 15 ppm nitrogen in N_4V^0 form by fitting an adapted $^{14}N_4V^0$ spectrum to the IR data. The total concentration of $^{15}N_3V^0$ generated by this processing regime was approximately 1.6(2) ppm, as measured by EPR. Photoluminescence (PL) measurements of the sample post-processing were dominated by N_3V^0, N_2V^0, N_2V^-, NV^0 and NV^-. The high levels of nitrogen aggregation at a moderate annealing temperature (1900 °C) are ascribed to the abundance of vacancies and interstitials introduced by the neutron irradiation [23].

2.2. Spectrometers

EPR measurements were performed on a Bruker EMX X-band spectrometer equipped with a ER 4109HS cylindrical resonator and an ER041XG microwave bridge: measurements were collected at non-

Table 1. The measured spin Hamiltonian parameters for the N_3V^0 defect. Parameters have been given for ^{14}N-doped diamond by scaling the measured ^{15}N hyperfine values by the ratio of the nuclear g-values $g_{14} : g_{15}$ ($g_{14} = 0.403\,761$ and $g_{15} = -0.566\,378$ [33]). The g-tensor values are calculated assuming that $^{14}N_s{}^0$ has an isotropic g-value of 2.0024. θ measured from [1 1 0] toward [0 0 1]; quadrupolar rhombicity given as $\eta = (P_x - P_y)/P_z$. Blanks in $^{15}N_3V^0$ parameters indicate values are as $^{14}N_3V^0$. A_{1-3} and $P_\parallel$ given in MHz.

	Zeeman			Hyperfine				Quadrupole		
	$g_\parallel$	$g_\perp$	$\theta(^\circ)$	A_1	A_2	A_3	$\theta(^\circ)$	$P_\parallel$	η	$\theta(^\circ)$
$^{14}N_3V^0$ [16]	2.0023(2)	2.0032(2)	35.26	7.4(1)	7.4(1)	11.2(1)	158(1)	−4.8(1)	0	145(2)
$^{14}N_3V^0$ (this work)	2.00241(5)	2.00326(5)	35.26	7.44(4)	7.46(4)	11.30(4)	157.8(2)	−4.73(5)	0	144.7(5)
$^{15}N_3V^0$ (this work)				−10.44(5)	−10.46(5)	−15.85(5)		— N/A —		

saturating microwave power. A PerkinElmer Spectrum GX Fourier-transform spectrometer was used to perform infrared (IR) absorption measurements, and a PerkinElmer Lambda 1050 spectrometer for ultraviolet-visible (UV-vis) absorption measurements.

The Lambda 1050 is a dispersive spectrometer, with light from a halogen bulb being monochromated before it is incident on the sample. The spectrometer compares the light intensity through two different paths (sample path, reference path) in order to determine the absorbance of the sample. Any light source which affects the two optical paths differently will therefore manifest as a baseline offset and must be excluded: this aspect is critical for our photochromism measurements, where a 100 mW green laser was used to excite the sample during the measurement. A ThorLabs FES0500 2.480 eV (500 nm) cut-off short-pass filter was employed to isolate the detector during the measurement. Testing with and without the laser revealed an absorbance offset of +0.05 (on 1.25 from the sample) at 2.755 eV (450 nm) under laser excitation.

The visible absorption of $N_s{}^0$ is a broad ramp starting at approximately 2.0 eV and increasing in intensity toward the ultraviolet (see underlying ramp of figure 1(c)) with a small feature at 4.59 eV (270 eV) [36]. The absorbance of this sample at >4.0 eV saturates our spectrometer, and hence any change in $N_s{}^0$ concentration will manifest only as a small baseline offset to the ramp. We cannot distinguish change this from laser leakage in the spectrometer (as discussed above) and therefore changes in $N_s{}^0$ were monitored by IR absorption, and N_3V^0 changes using visible absorption.

2.3. Spin Hamiltonian

The spin Hamiltonian for a single electron, multiple nucleus system is given by

$$\mathbf{H} = \mu_B \mathbf{B}^T \cdot \underline{\mathbf{g}} \cdot \mathbf{S} + \sum_i^N \mathbf{S}^T \cdot \underline{\mathbf{A}}_i \cdot \mathbf{I}_i + \mathbf{I}_i^T \cdot \underline{\mathbf{Q}}_i \cdot \mathbf{I}_i \ ,$$

with i summed over the nuclei. These terms represent the electronic Zeeman, electron-nuclear hyperfine, and nuclear quadrupole interactions, respectively. Applying a magnetic field lifts the degeneracy of the electronic states m_S via the Zeeman interaction, with transitions between the states driven by resonant high frequency magnetic fields (usually in the microwave region) — the electron paramagnetic resonance phenomenon. Each nucleus splits the electron resonance line into $2I + 1$ lines, where I is the nuclear spin of the isotope in question: 1 for ^{14}N; 1/2 for ^{15}N. For an arbitrary magnetic field $\mathbf{B}$ applied to N_3V^0 we therefore expect $3^3 = 27$ ($2^3 = 8$) lines per symmetry-related orientation for the ^{14}N (^{15}N) case. The ^{14}N case is further complicated by the quadrupolar interaction, which is only non-zero for $I > 1/2$: this interaction enables so-called "forbidden" ($\Delta m_S = 1$; $\Delta m_I \neq 0$) transitions to acquire appreciable intensity, and can yield up to $27^2 = 729$ lines per symmetry-related orientation. The ^{15}N case is therefore spectrally significantly less complex to interpret, yet can determine 7 of the 10 spin Hamiltonian parameters for the ^{14}N spectrum.

3. Results

3.1. EPR

A typical EPR spectrum of the sample with an applied magnetic field $\mathbf{B} \| \langle 0\,0\,1 \rangle$ is given in figure 2. $^{15}N_3V^0$ was identified by modifying the published Hamiltonian parameters for $^{14}N_3V^0$: the hyperfine interaction strengths were scaled by the ratio of the isotopic nuclear g-values ($g_{14} = 0.403\,761$ and $g_{15} = -0.566\,378$ [33]) and the quadrupolar interaction was removed.

Unlike the ^{14}N spectrum (Fig. 1(a)), the interpretation of the $^{15}N_3V^0$ spectrum is relatively simple (figure 2). As a consequence of the C_{3v} symmetry of the defect, all four symmetry-related orientations are equivalent when the external magnetic field is applied along $\langle 0\,0\,1 \rangle$ and only one g-value is observed. Furthermore, the hyperfine interaction for each nitrogen nucleus is also identical, and for three equivalent $I = 1/2$ nuclei at an $S = 1/2$ centre, a 1:3:3:1 intensity pattern is expected. In fact, the approximate pattern is 1:1:2:2:1:1, with the highest-intensity lines split by

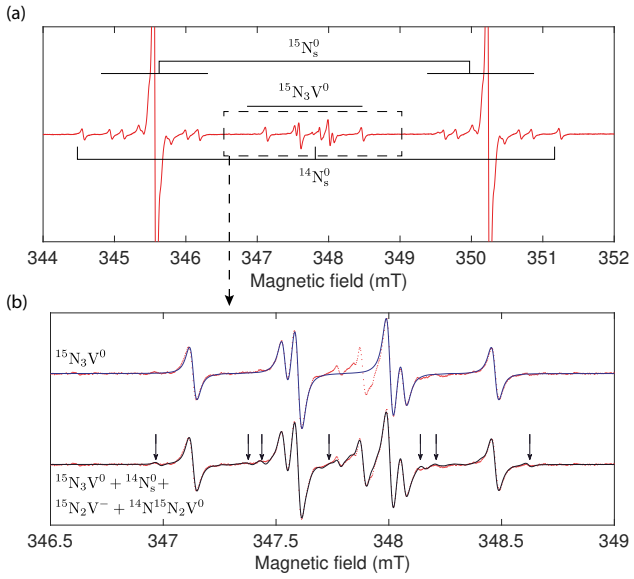

Figure 2. (a) Measured EPR spectrum of synthetic ^{15}N-doped HPHT-treated sample with applied magnetic field $B\|\langle 0\,0\,1\rangle$. Three paramagnetic systems are visible and labeled. The $^{15}N_3V^0$ EPR spectrum is significantly simpler than the ^{14}N analogue (Fig. 1(a)). (b) Zoom of marked area in (a). Top: Experimental spectrum (dotted) and generated $^{15}N_3V^0$ spectrum (solid). Bottom: Experimental (dotted) and generated spectrum including $^{14}N_s^0$, $^{15}N_3V^0$, $^{15}N_2V^-$, and an N_3V center consisting of one ^{14}N and two ^{15}N nuclei ($^{14}N^{15}N_2V^0$): prominent resonances for this spectrum are highlighted with arrows. The relative intensities of $^{15}N_3V^0$:$^{14}N^{15}N_2V^0$ are consistent with the source nitrogen isotopic ratio.

second-order hyperfine effects. As expected, the spectrum is significantly simpler than in the ^{14}N case.

Further spectra were measured with the applied magnetic field along $\langle 1\,1\,0\rangle$ and $\langle 1\,1\,1\rangle$, in addition to $\langle 0\,0\,1\rangle$. The spectra for all three orientations were fitted simultaneously: the obtained spin Hamiltonian parameters are given in Table 1. The revised $^{15}N_3V^0$ spin Hamiltonian parameters were then used to improve the fit for $^{14}N_3V^0$, where the only free parameters are those relating to the quadrupole interaction.

A second (natural) diamond with natural nitrogen isotope abundance (100 % ^{14}N), and containing approximately 25 ppm of $^{14}N_3V^0$ was studied. Once again, EPR spectra of three high-symmetry directions were measured and simultaneously fitted. The updated spin Hamiltonian parameters enable fitting of the $^{14}N_3V^0$ spectrum along arbitrary directions (see figure 3). It is interesting to note that the updated parameters all lie within the quoted errors of the published data; however, the spectrum is complex due to several interactions of similar magnitudes, and hence very small relative changes in the hyperfine, quadrupole and Zeeman interactions have a dramatic effect on the generated spectrum.

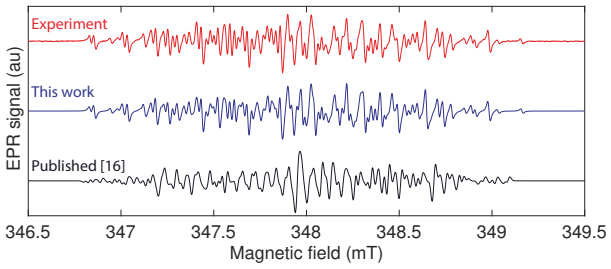

Figure 3. EPR spectrum of a natural diamond with applied magnetic field $B\|\langle 1\,1\,1\rangle$. Top to bottom: experimental data; spectrum generated using the spin Hamiltonian parameters given in table 1; spectrum generated using the spin Hamiltonian parameters given in [16]. The calculated N_s^0 spectrum was subtracted from the experimental data before fitting.

3.2. Photochromism

The negative charge states of NV and N_2V have both been identified; however, no negative analogue of N_3V^0 has been identified by EPR, optical absorption or PL. Indirect evidence for N_3V^- was obtained in material with high N_s^0 by monitoring the ZPL of N_3V^0 at 2.988 eV) (415 nm) in absorption while pumping with a filtered arc lamp: upon illumination with light of energy >1.65 eV the ZPL was seen to increase [37]. This energy was interpreted as the ionization threshold for N_3V^-: as only the N_3V^0 ZPL was monitored, no corresponding donor (or acceptor) was identified. No effect was observed when the same experiment was performed in material with low single nitrogen concentration.

Measurements of the sample at 110 K show an increase in N_3V^0 of approximately 0.1 ppm (using the calibration coefficient in [39]) when illuminated by 100 mW at 2.33 eV (532 nm, Fig 4(a)). Measurements in the infrared record changes in N_s^+ and N_s^0 of $-1.3(1)$ ppm and $+1.3(5)$ ppm, respectively, when the sample is illuminated with 100 mW at 2.36 eV (525 nm, Fig. 4(b)). Taken together, these results suggest that illumination drives the process

$$(N_3V^- + N_s^+ \rightarrow N_3V^0 + N_s^0)\,. \qquad (1)$$

The excitation energies employed here are close to the photoionization threshold of N_s^0 (approximately 1.9–2.2 eV [40, 41]). The energy for $N_s^+ + \nu \rightarrow N_s^0 + h^+$ is 4.0 eV [42] and hence we cannot drive this process in our experiments. We therefore infer that our optical excitation is leading to ionization of N_3V^- directly, and during illumination we are driving process (1) in both the forward and backward direction due to consecutive ionization of N_3V^- and N_s^0.

The historical lack of observation of N_3V^- is not unexpected: N_3V represents significant nitrogen aggregation in diamond, and it is unusual to observe high-order aggregates and single substitutional

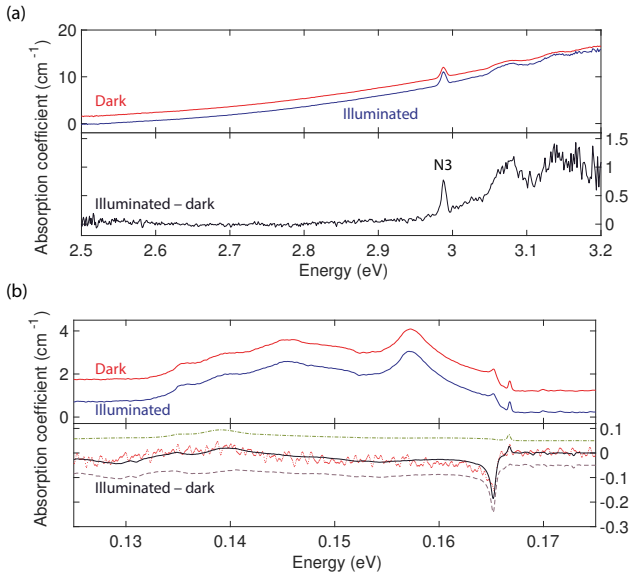

Figure 4. (a) UV-Vis absorption spectra of the ^{15}N-doped sample at 110 K. Top: spectra collected with and without 100 mW illumination at 2.33 eV (532 nm). Dark spectrum offset by 1 cm^{-1} for clarity. Bottom: difference spectrum: there is a clear increase in the N3 ZPL and associated vibronic band under illumination. (b) The one-phonon infrared absorption spectrum of the ^{15}N-doped sample at 110 K. Top: spectra collected with and without 100 mW illumination at 2.36 eV (525 nm). Dark spectrum offset by 1 cm^{-1} for clarity. Bottom: difference spectrum (experimental, dots) and fit (solid line). The fit was generated by performing least squares fitting of ^{15}N reference spectra for N_s^+ (dashed line) and N_s^0 (dash-dot). The sum spectrum represents a change of $\Delta[N_s^+] = -1.3(1)$ ppm [38] and $\Delta[N_s^0] = +1.3(5)$ ppm using absorption oscillator coefficients of 5.5 ppm cm^{-1} at 165.2 meV (1332 cm^{-1}) [38] and 37 ppm cm^{-1} at 166.6 meV (1344 cm^{-1}) [35].

nitrogen in the same sample, as required for the initial $N_s \leftrightarrow N_3V$ process to occur. The identification of the donor in this process as N_s^0 combined with previous ionization results [37] indicates that the photoionization threshold for N_3V^- lies in the range 1.65–2.2 eV.

Evidently the change in N_3V^0 concentration cannot account for the entirety of the charge transfer. We expect the processes ($N_2V^- + N_s^+ \rightarrow N_2V^0 + N_s^0$) and ($NV^- + N_s^+ \rightarrow NV^0 + N_s^0$) to be occurring simultaneously: unfortunately, both charge states of NV were below absorption detection limits; and the bandblock filter used to exclude the laser light from the spectrometer also blocks the ZPL of both charge states of N_2V. Subsequent absorption measurements in the range 1.37–2.18 eV (900–570 nm) did not identify any sharp features with or without illumination.

4. Conclusion

Recent advances in synthesis and processing have enabled us to create a sample with a significant quantity of $^{15}N_3V^0$. Due to the dramatic simplification of the ^{15}N spectrum we have been able to refine the spin Hamiltonian parameters of both $^{15}N_3V^0$ and $^{14}N_3V^0$: this enables the fitting and hence EPR-based quantification of N_3V^0 with the sample in an arbitrary orientation relative to the applied magnetic field. Subsequent optical absorption measurements of the ^{15}N-doped sample under illumination have indicated charge transfer between substitutional nitrogen N_s and N_3V. The simplest model consistent with our results suggests the presence of the as-yet unobserved charge state N_3V^-. Careful absorption and photoluminescence measurements in the 1.65–2.2 eV range may identify features associated with N_3V^-.

References

[1] Le Sage D, Arai K, Glenn D R, DeVience S J, Pham L M, Rahn-Lee L, Lukin M D, Yacoby A, Komeili A and Walsworth R L 2013 *Nature* **496** 486–9
[2] Barry J F, Turner M J, Schloss J M, Glenn D R, Song Y, Lukin M D, Park H and Walsworth R L 2016 *Proc. Natl. Acad. Sci.* **113** 201601513
[3] Sun H, Simon R B, Pomeroy J W, Francis D, Faili F, Twitchen D J and Kuball M 2015 *Appl. Phys. Lett.* **106** 111906
[4] Pomeroy J W, Bernardoni M, Dumka D C, Fanning D M and Kuball M 2014 *Appl. Phys. Lett.* **104** 083513
[5] Maclean A J, Kemp A J, Calvez S, Kim J Y, Kim T, Dawson M D and Burns D 2008 *IEEE J. Quantum Electron.* **44** 216–225
[6] Sumiya H 2012 *Sumitomo Electr. Tech. Rev.* 15–23
[7] Zamboni I, Pastuović Ž and Jakšić M 2013 *Diam. Relat. Mater.* **31** 65–71
[8] Peaker C V, Atumi M K, Goss J P, Briddon P R, Horsfall A B, Rayson M J and Jones R 2016 *Diam. Relat. Mater.* **70** 118–123
[9] Evans T and Qi Z 1982 *Proc. R. Soc. London Ser. A* **381** 159–178
[10] Felton S, Edmonds A M, Newton M E, Martineau P M, Fisher D and Twitchen D J 2008 *Phys. Rev. B* **77** 081201
[11] Felton S, Edmonds A M, Newton M E, Martineau P M, Fisher D, Twitchen D J and Baker J M 2009 *Phys. Rev. B* **79** 075203
[12] Doherty M W, Manson N B, Delaney P, Jelezko F, Wrachtrup J and Hollenberg L C L 2013 *Phys. Rep.* **528** 1–45
[13] Loubser J H N and van Wyk J A 1981 Models for the H3 and H4 centres based on ESR measurements *32nd Diam. Conf.* (Reading: Diamond Conference)
[14] Green B L, Dale M W, Newton M E and Fisher D 2015 *Phys. Rev. B* **92** 165204
[15] Davies G, Welbourn C and Loubser J H N 1978 *Diam. Res.* 23–30
[16] van Wyk J A and Loubser J H N 1993 *J. Phys. Condens. Matter* **5** 3019–3026
[17] Collins A T 2003 *Diam. Relat. Mater.* **12** 1976–1983
[18] Farrer R G 1969 *Solid State Commun.* **7** 685–688
[19] Welbourn C, Cooper M and Spear P 1996 *Gems Gemol.* **32** 156
[20] van Wyk J A 1982 *J. Phys. C Solid State Phys.* **15** L981–L983
[21] Mainwood A 1994 *Phys. Rev. B* **49** 7934–7940
[22] Papagiannidis S 2003 *Ab initio modelling of defect complexes in semiconductors* Ph.D. thesis University of Newcastle upon Tyne

[23] Collins A T 1980 *J. Phys. C Solid State Phys.* **13** 2641–2650
[24] Goss J, Briddon P, Papagiannidis S and Jones R 2004 *Phys. Rev. B* **70** 235208
[25] Jones R, Goss J P, Pinto H and Palmer D W 2015 *Diam. Relat. Mater.* **53** 35–39
[26] Pinto H, Jones R, Palmer D W, Goss J P, Briddon P R and Öberg S 2012 *Phys. status solidi* **209** 1765–1768
[27] Collins A T, Connor A, Ly C H, Shareef A and Spear P M 2005 *J. Appl. Phys.* **97** 083510–083517
[28] Chrenko R M, Tuft R E and Strong H M 1977 *Nature* **270** 141–144
[29] Liggins S, Newton M E, Goss J P, Briddon P R and Fisher D 2010 *Phys. Rev. B* **81** 1–7
[30] Dale M W 2015 *Colour centres on demand in diamond* Ph.D. thesis University of Warwick
[31] Coulson C and Kearsley M 1957 *Proc. R. Soc. A Math. Phys. Eng. Sci.* **241** 433–454
[32] Jones R, Goss J, Briddon P and Öberg S 1997 *Phys. Rev. B* **56** R1654–R1656
[33] Stone N 2005 *At. Data Nucl. Data Tables* **90** 75–176
[34] Strömann C, Vera H, Tshisikhawe F, Hansen J and Burns R 2006 Synthesis of Diamond
[35] Liggins S 2010 *Identification of point defects in treated single crystal diamond* Ph.D. thesis University of Warwick
[36] Khan R U A, Martineau P M, Cann B L, Newton M E and Twitchen D J 2009 *J. Phys. Condens. Matter* **21** 364214
[37] Mita Y, Kanehara H, Nisida Y and Okada M 1997 *Philos. Mag. Lett.* **76** 93–98
[38] Lawson S C, Fisher D, Hunt D C and Newton M E 1998 *J. Phys. Condens. Matter* **10** 6171–6180
[39] Davies G 1999 *Phys. B Condens. Matter* **273-274** 15–23
[40] Heremans F J, Fuchs G D, Wang C F, Hanson R and Awschalom D D 2009 *Appl. Phys. Lett.* **94** 152102
[41] Isberg J, Tajani A and Twitchen D J 2006 *Phys. Rev. B - Condens. Matter Mater. Phys.* **73** 245207
[42] Jones R, Goss J and Briddon P 2009 *Phys. Rev. B* **80**